4D seismic quantification of a growing CO_2 plume at Sleipner, North Sea

R. A. CHADWICK,[1] R. ARTS[2] and O. EIKEN[3]

[1] *British Geological Survey, Kingsley Dunham Centre, Keyworth, Nottingham, NG12 5GG, UK (e-mail: rach@bgs.ac.uk)*
[2] *Netherlands Institute of Applied Geoscience TNO – National Geological Survey, Princetonlaan 6, PO Box 80015, 3508 TA Utrecht, The Netherlands*
[3] *Statoil Research Centre, Rotvoll, N-7005 Trondheim, Norway*

Abstract: CO_2 produced at the Sleipner natural gas field is being injected into the Utsira Sand, a major saline aquifer. Time-lapse seismic data were acquired in 1999 and 2001, with 2.35 and 4.26 million tonnes of CO_2 in the reservoir respectively. The CO_2 plume is imaged as a number of bright sub-horizontal reflections within the reservoir unit, growing with time, and underlain by a prominent velocity pushdown. No leakage has been detected from the repository reservoir. The reflections are interpreted as tuned responses from thin (<8 m thick) layers of CO_2 trapped beneath thin intra-reservoir mudstones and the reservoir caprock. However, these alone are unable to account for the amount of observed pushdown. A two-component 3D saturation model is therefore developed for the 1999 dataset, with high-saturation CO_2 forming the layers and a lesser component of low-saturation CO_2 between the layers. Saturations are calculated from the observed reflectivity and velocity pushdown and the resulting model contains 85% of the known injected mass of CO_2. A 2D synthetic seismic section through the saturation model matches the observed seismic response well and the model is considered to provide an acceptable description of the CO_2 distribution. Signal attenuation is more pronounced within the 2001 plume and its effects are likely to become more significant with time, perhaps reducing the efficacy of seismic verification techniques as the plume grows further. Other geophysical methods, such as microgravimetry, may become increasingly useful at this stage.

Keywords: carbon dioxide, storage, sequestration, seismic, time-lapse, Sleipner Field, greenhouse effect

The carbon dioxide injection operation at the Sleipner gas field in the North Sea (Baklid *et al*. 1996), operated by Statoil and the Sleipner partners, is the world's first industrial scale CO_2 injection project designed specifically as a greenhouse gas mitigation measure. CO_2 separated from natural gas produced at Sleipner is currently being injected into the Utsira Sand, a major saline aquifer some 26 000 km^2 in area (Fig. 1). Injection started in 1996 and is planned to continue for about twenty years, at a rate of about one million tonnes per year.

The SACS project and its successor CO2STORE run in parallel with the ongoing injection operation. Their objectives are to monitor and model the injected CO_2 in order to demonstrate that underground storage is a safe and verifiable technology in the long term. More specifically, the time-lapse seismic surveys aim to demonstrate storage integrity (and to provide early warning should any leakage occur), to monitor the migration and dispersal of the CO_2 plume, to calibrate and verify short-term reservoir simulations and to assist in the development of long-term predictive models. A further aim is to test the efficacy of time-lapse seismic as a quantification and verification tool in the event that subsequent CO_2 storage operations will have to demonstrate compliance with future regulatory requirements.

Baseline 3D seismic data were acquired in 1994, prior to injection. A first repeat survey, covering some 26 km^2, was acquired in October 1999, with 2.35 million tonnes of CO_2 in the reservoir, and a second repeat survey was acquired in September 2001 with 4.26 million tonnes of CO_2 *in situ*. This paper describes some of the findings from the three surveys. These include vivid 4D seismic images of the growing CO_2 plume, an improved CO_2 saturation model for the 1999 plume, and an assessment of the issues involved in quantifying the amount of CO_2 in the reservoir.

This paper is restricted to analysis of the post-stack data. Pre-stack analysis is being carried out in parallel and will be the subject of future publications.

Background to the injection operation

CO_2 is being injected into the Utsira reservoir via a deviated (near-horizontal) well, through a 38 m long well perforation interval 1010–1013 m below sea level (bsl), and about 2.3 km from the drilling platform. The injection point is close to the base of the Utsira Sand, about 200 m below the reservoir top, and beneath a gentle domal closure of some 12 m relief. At the time of writing there are more than 6 million tonnes of CO_2 *in situ*.

Properties of the Utsira Sand reservoir

The Utsira Sand forms part of the Mio-Pliocene Utsira Formation (Gregersen *et al*. 1997; Chadwick *et al*. 2001, 2003). It is axially situated within the thick post-rift succession of the northern North Sea Basin, forming a basin-restricted lowstand deposit of considerable extent, over 400 km from north to south and typically 50–100 km west to east. Sleipner lies towards the southern limit of the Utsira Sand (Fig. 1), where the reservoir is 800–1000 m deep and 200–300 m thick. Core measurements, petrographic analysis and well logs (Zweigel *et al*. 2001, 2004), show the sand to be clean and largely uncemented with porosities in the range 0.30–0.42 (here a mean value of 0.37 is taken). Geophysical well logs from the Sleipner area resolve thin beds of intra-reservoir mudstone or shale, characterized by high gamma-ray readings (Fig. 2). These are laterally impersistent and cannot generally be correlated from well to well. Thicknesses typically range from less than a metre to more than two metres, with a well-defined modal peak at just over one metre (Zweigel *et al*. 2001). In the Sleipner area, a thicker,

CHADWICK, R. A., ARTS, R. & EIKEN, O. 2005. 4D seismic imaging of a CO_2 plume. *In*: DORÉ, A. G. & VINING, B. A. (eds) *Petroleum Geology: North-West Europe and Global Perspectives—Proceedings of the 6th Petroleum Geology Conference*, 1385–1399.

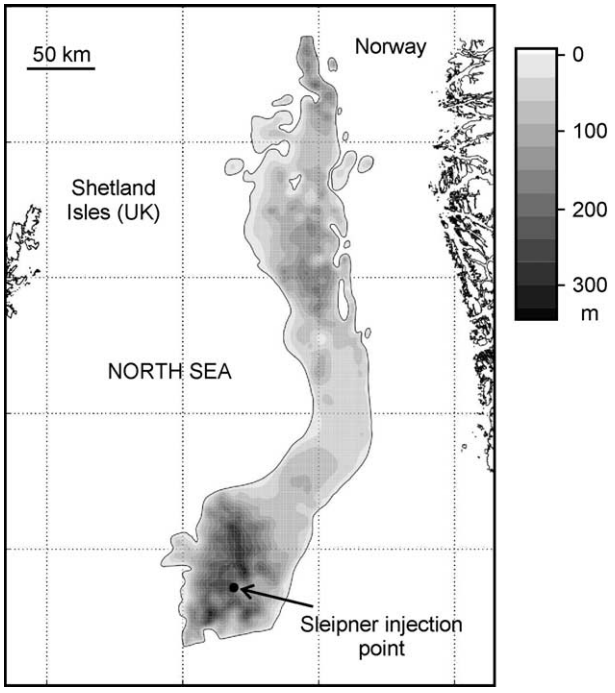

Fig. 1. Limits and thickness of the Utsira Sand and location of the Sleipner injection point.

more laterally extensive mudstone, some 5 m thick (here termed the 'five-metre mudstone') separates the uppermost sand unit from the main reservoir sand beneath (Fig. 2). The shale layers constitute important permeability barriers within the reservoir sand, and have proved to have a significant effect on CO_2 migration through, and entrapment within, the reservoir. However, the fact that the strongly deviated injection well penetrates the top of the Utsira Sand some 1.3 km WSW of the injection point means that an accurate reservoir model is not available for the immediate vicinity of the CO_2 plume. Because of this the structural disposition of the mudstone layers is not known (see below).

The Utsira Sand is overlain by the Nordland Formation (Isaksen & Tonstad 1989), which mostly comprises prograding deltaic wedges of Pliocene age. These generally coarsen upwards, from mudstones in the deeper, axial parts of the basin, to silt and sand in the shallower and more marginal parts. In the Sleipner area, the lowest unit, a 50–100 m thick silty mudstone, forms the immediate reservoir caprock.

Acoustic properties of the CO_2-water-rock system

The current CO_2 plume lies between the injection point at 1012 m and the top of the reservoir at about 800 m bsl. Key physical properties of the reservoir system are summarized in Table 1. Formation temperatures are based on a single downhole measurement at Sleipner, and are therefore subject to some uncertainty. Lower formation temperatures than the measured value would have little impact, but if temperatures were significantly (>5 °C) higher, CO_2 densities would be significantly reduced. This would impact on the quantification analysis. Scattered pressure measurements for the Utsira Sand indicate that regional formation pressures are hydrostatic. Moreover, the lack of any systematic increase in measured injection pressure at the surface indicates that no rise in formation pressure has so far occurred. CO_2 properties are based on density and velocity information commissioned by Statoil, other published information, and solution of an equation of state (Span & Wagner 1996). Suffice to say that within the current plume, the CO_2 forms a compressible but buoyant 'supercritical' fluid, of low viscosity and high mobility. Its density is probably slightly higher at the top of the reservoir because the lower temperature outweighs the reduced pressure (Lindeberg 1996). The effect of minor known impurities such as methane would permit lower densities than those calculated for pure CO_2, and, for the purposes of this paper, a value of 700 kgm^{-3} is taken. The calculated volumes of *in situ* CO_2 are also given in Table 1. Irrespective of the precise reservoir conditions, the principal driving force for the migration of CO_2 up through the reservoir is buoyancy, due to the density difference, $\Delta\rho$, between CO_2 and brine. From a geochemical standpoint, reaction of the CO_2 with the reservoir sand is minimal (e.g. Pearce *et al*. 2001), but CO_2 may well react with the intra-reservoir mudstones in the medium to long term (e.g. Johnson & Nitao 2003).

The Gassmann equations (Gassmann 1951) were used to calculate seismic velocities in rock containing CO_2 at various saturations using S- and P-wave velocity information from Sleipner and published elastic property data (Table 1). Velocities decrease from the observed value of about 2050 ms^{-1} in water-saturated sand, to about 1420 ms^{-1} in wholly CO_2 saturated sand

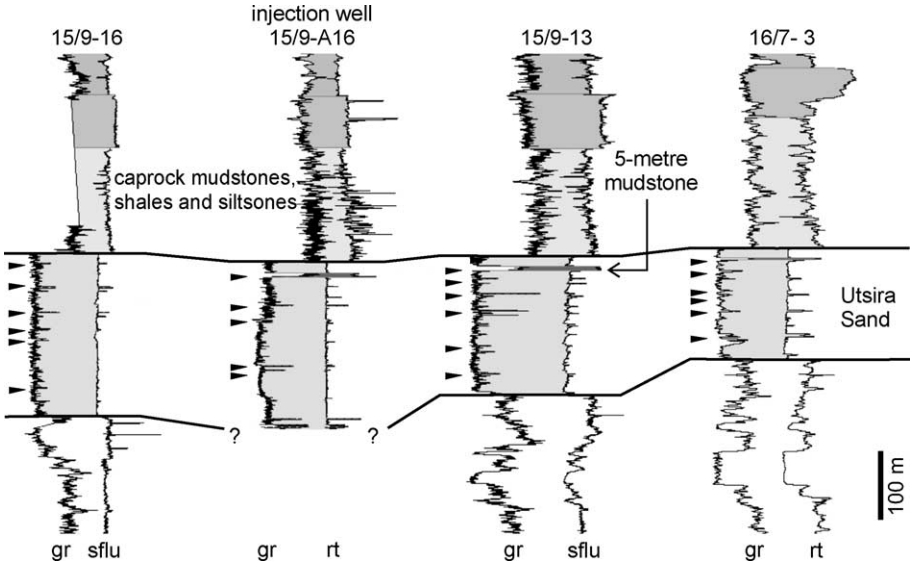

Fig. 2. Geophysical logs in wells close to Sleipner. The Utsira Sand has much lower gamma-ray (gr) signature than the caprock succession. Gamma-ray peaks within the sand (main peaks arrowed) are interpreted as thin beds of mudstone. Note the injection well is strongly deviated and the drilled sequence will differ from that at the plume location.

Table 1. Reservoir and fluid properties and *in situ* amounts of CO_2 at the times of the 1999 and 2001 surveys. All properties are at reservoir conditions (reservoir properties based on well log data, supported by core analysis)

	Depth (m)	Assumed temperature (°C)	Pressure (MPa)	Density CO_2 (kgm^{-3})	Seismic velocity CO_2 (ms^{-1})	Bulk modulus CO_2 (MPa)	*In Situ* mass of CO_2 (kg) ($\times 10^9$)	Estimated *in situ* volume of CO_2 (m^3) ($\times 10^6$)
Top Utsira Sand	825	29	8.6	744	335	0.083	2.35*	3.36*
Injection point	1012	36	10.5	718	330	0.076	4.26†	6.09†

V_p Utsira Sand (water-saturated) 2050 ms^{-1} (range 1950 to 2100 ms^{-1}), V_s Utsira Sand (water-saturated) 640 ms^{-1} (range 600 to 680 ms^{-1}), Porosity Utsira Sand 0.37 (range 0.32 to 0.42), Density Utsira Sand (water-saturated) 2050 kgm^{-3} (range 1960 to 2080 kgm^{-3}), Density Utsira pore-water 1040 kgm^{-3}, Density of CO_2 in reservoir 700 kgm^{-3}, Bulk modulus of quartz 36.9 GPa, Bulk modulus of water 2.305 GPa, Bulk modulus of CO_2 0.08 GPa.
* 1999 Survey.
† 2001 Survey.

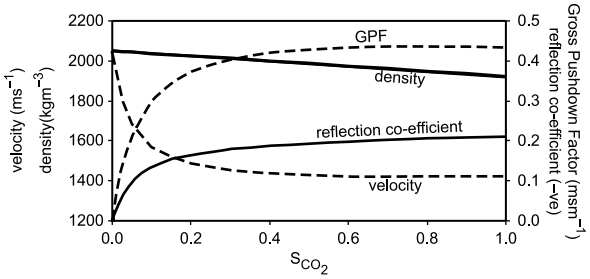

Fig. 3. Properties of the CO_2–water–rock system showing variation in velocity, density, reflection co-efficient (with respect to water-saturated sand) and Gross Pushdown Factor.

(Fig. 3). It is notable that much of this decrease develops at low CO_2 saturations with the consequence that, volume-for-volume, low-saturation CO_2 is a much more effective pushdown agent than CO_2 at high saturations (Chadwick *et al*. 2004). This introduces an inherent uncertainty into any modelling technique that seeks to invert observed pushdown into a CO_2 saturation distribution. Errors are related mostly to uncertainties in elastic parameters, principally the bulk moduli of the rock framework and of fluid CO_2. The Gassmann equations assume a homogeneous mix of fluids, and a more patchy distribution would give a more nearly linear velocity–saturation relationship. Direct observation of velocity pushdown within the plume, suggests, however, that the calculated velocities are not significantly in error (Chadwick *et al*. 2004). Pressure effects on the seismic velocities are expected to be negligible, since no systematic increase in injection pressure has so far been observed during the injection process. Using the Gassmann velocities and calculated densities (Fig. 3), the acoustic impedance of rock filled with CO_2 at various saturations was also calculated. From this, reflection coefficients between water-saturated rock and CO_2-saturated rock were computed, with values of around -0.2 over a range of CO_2 saturations (Fig. 3).

Reflectivity of the CO_2 plume

The 1994 pre-injection data (Fig. 4a) show reflections of moderate amplitude from the top and base of the reservoir, the more complex (triplet) reflection pattern at the reservoir top deriving from interference with the underlying 'five-metre mudstone' bed. Intra-reservoir events are much weaker and largely obscured by noise. In particular the reflection at mid-Utsira level is a seabed multiple of the stronger events near to the top of the reservoir. The apparent antiformal stratal geometries, sub-parallel to the top reservoir surface, may therefore be artefacts. The fact that the different CO_2 accumulations have radically different shapes, suggests control by more complex bedding geometries within the reservoir unit.

As predicted from the calculated reflection coefficients, introducing CO_2 into the Utsira reservoir has a dramatic effect on reflectivity. The 1999 data show a clear image of the CO_2 plume with strong reflections at a number of discrete levels within the reservoir. The 2001 data show further development of the CO_2 plume, particularly in its upper part, with lateral growth of the horizons identified on the 1999 data. The integrated reflection amplitude data (Fig. 4b) show the plume to be markedly elliptical in plan, elongated NNE–SSW, with a major axis increasing from about 1.8 km in 1999 to 2.4 km in 2001. The minor axis of about 0.9 km has remained roughly constant between 1999 and 2001, with the eastern boundary of the plume staying more-or-less fixed with, by 2001, the development of a markedly linear edge.

Nine reflection horizons have been identified in the plume, ranging from Horizon 1, some 50 m above the injection point, to Horizon 9 at the topmost surface of the reservoir. All horizons can

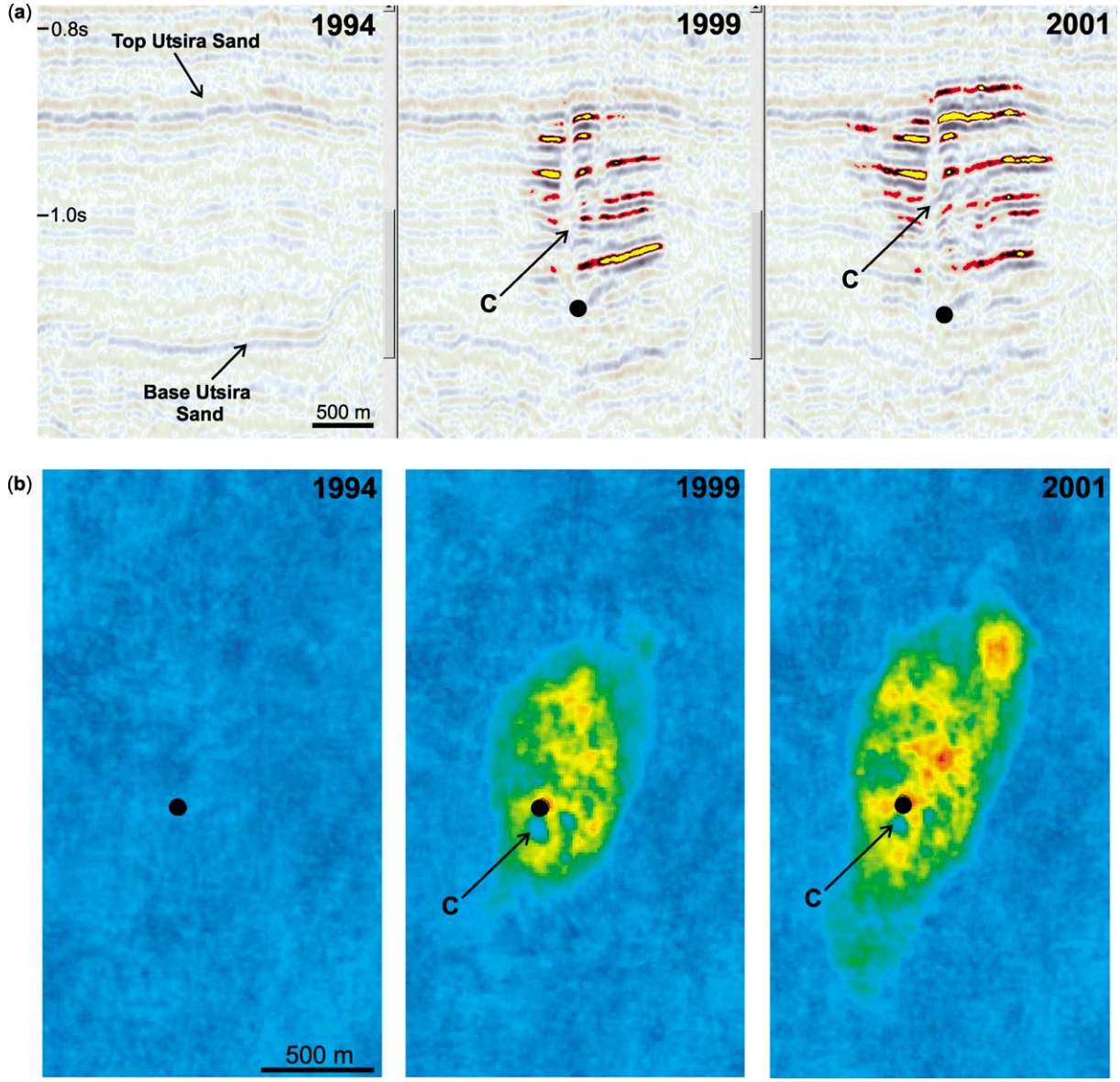

Fig. 4. Time-lapse seismic images of the CO_2 plume (**a**) N–S inline through the 1994 dataset prior to injection and through the 1999 and 2001 datasets. Enhanced amplitude display with red/yellow denoting a negative reflection coefficient. (**b**) Maps of integrated absolute reflection amplitudes calculated in a twtt window from 0.84 to 1.08 s. Blue, low reflectivity; red, high reflectivity. Black disc denotes injection point. C denotes the main chimney.

be identified on both the 1999 and 2001 data (Fig. 5). The probable presence of multiple energy, and the likelihood of plume reflections representing composite interference wavelets, mean that other interpretations with a different number of horizons cannot be discounted (*cf.* Chadwick *et al*. 2004). The horizons were picked on wavelet troughs, signifying negative acoustic impedance contrasts, and are interpreted as corresponding closely to the tops of layers containing CO_2 that has accumulated or 'ponded' beneath the thin, intra-reservoir mudstones. As discussed above, the lack of well data through the plume itself means that the observed reflection horizons cannot be directly correlated with proven mudstone layers. Because the horizons have markedly different lateral extents and are not all mutually overlapping, at any given locality, between five and seven horizons are typically present. This is roughly consistent with the number of mudstone layers (including the topseal) indicated in the wells (Fig. 2).

The CO_2 related reflections do not show the gentle antiformal or near flat-lying geometry of the Utsira stratigraphy as suggested by the 1994 data, but rather show a downward pointing V-profile, which becomes more pronounced downwards through the reservoir. This is interpreted as an effect of velocity pushdown within the plume (Arts *et al*. 2002; Chadwick *et al*. 2004).

Vertical linear zones within the plume, characterized by reduced reflection amplitudes and localized pushdown, are interpreted as 'chimneys' of moderate or high CO_2 saturation. The main chimney is particularly prominent and is visible above, but just to the south of, the injection point (Figs 4a,b). Described in more detail by Chadwick *et al*. (2004), it is interpreted as the main conduit for CO_2 upward migration in the plume, and the principal feeder of the laterally expanding thin layers.

Thin-layer effects

The total *in situ* volumes of CO_2 in 1999 and 2001 were 3.36×10^6 and $6.09 \times 10^6\,m^3$ respectively (Table 1). These correspond to total plan areas of the nine horizons, in 1999 and 2001, of $3.04\,km^2$ and $5.07\,km^2$ respectively. If all of the CO_2 in the plume were trapped within these layers, and taking a mean reservoir porosity of 0.37, the layers would, on average, be only about 2.99 m thick in 1999 and 3.25 m thick in 2001. Given that a significant proportion of the CO_2 in the plume is likely to be present at low saturations in between the layers (see below), average layer thicknesses are likely to be even less than this, and certainly generally beneath the limit of seismic bed-thickness resolution ($\lambda/4$, ~8 m for these

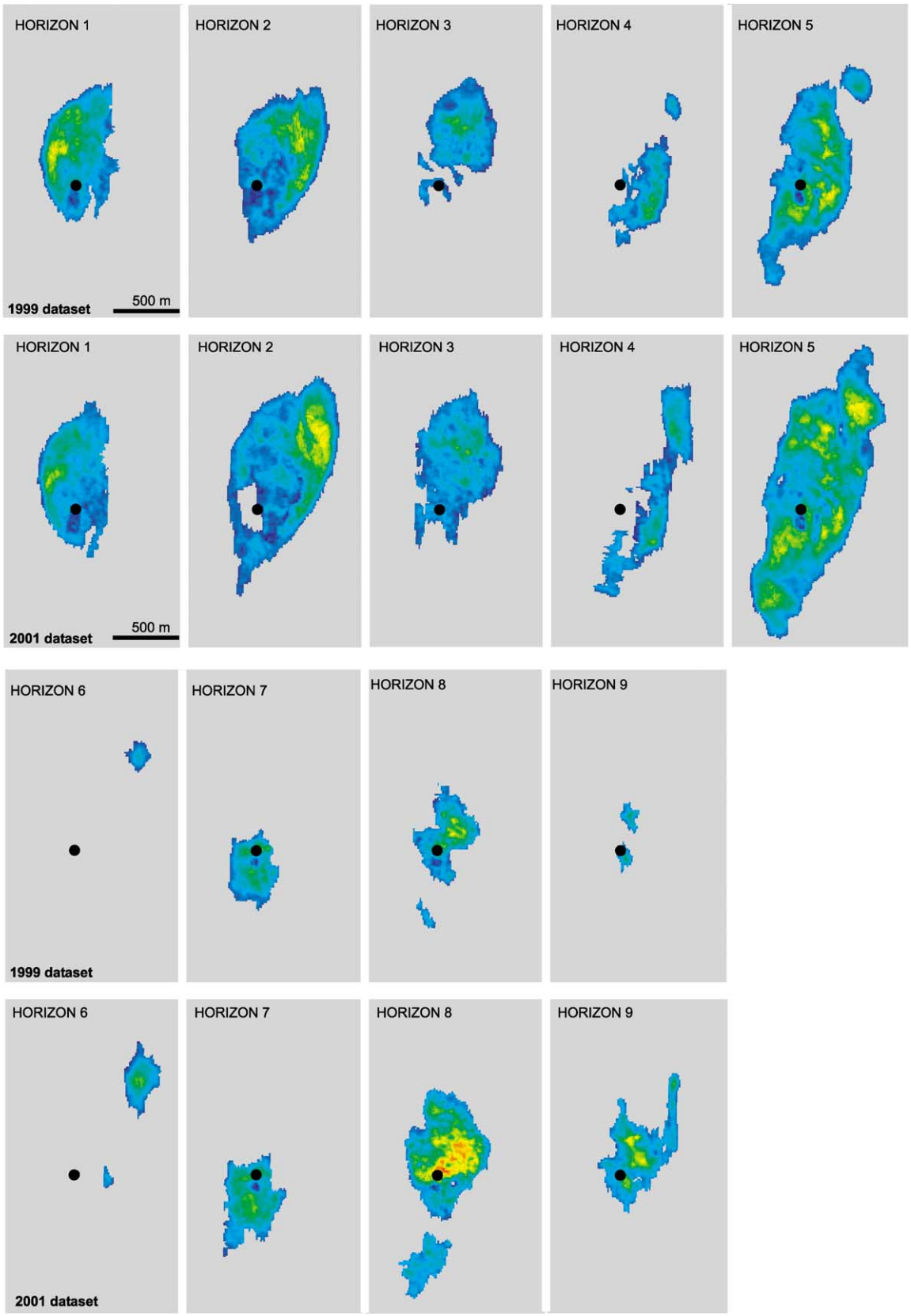

Fig. 5. Plume development 1999–2001. Absolute amplitude maps of the interpreted horizons on the 1999 (top) and 2001 (bottom) surveys. Black disc denotes injection point.

data). The observed CO_2 reflectivity is, therefore, largely a consequence of thin-layer interference. For thin layers, reflection amplitude is related directly to layer thickness, increasing from zero at zero layer thickness, to a maximum at the tuning thickness (Arts *et al*. 2003). This is illustrated by simple convolution modelling (Fig. 6). Convolution takes no account of pre-stack amplitude – offset effects, but full elastic modelling of CMP gathers from the Sleipner datasets lends support to the near-linear amplitude – thickness relationship (Svend Østmo, pers. comm.). Thus, observed amplitudes on the picked horizons which tend

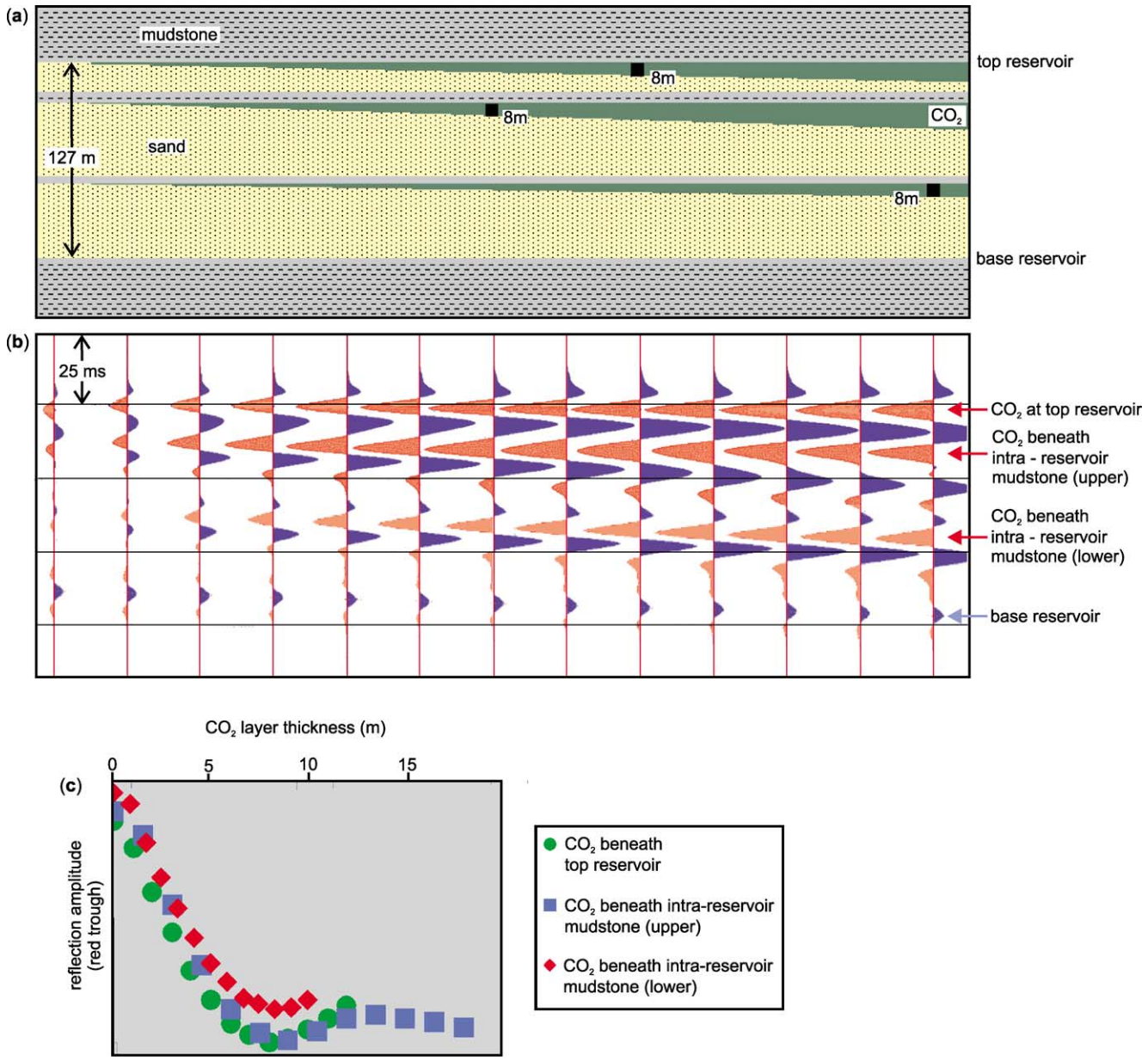

Fig. 6. (**a**) Illustrative reservoir model with mudstones of various thickness overlying rightward thickening layers of CO_2-saturated sand. (**b**) Seismic response of the above model convolved with a zero-phase wavelet statistically derived from the Sleipner data windowed on the Utsira Sand (red troughs denote negative reflection coefficients). Reflection energy increases rightwards from zero, peaking at layer thicknesses of about 8 m. Note velocity pushdown (~9 ms) at base reservoir. (**c**) Relationship of amplitude to thickness for the three CO_2 layers. Minor amplitude variations reflect the differing thicknesses of the overlying mudstone layers, the mean tuning thickness is about 8.2 m.

to increase systematically inwards, from zero at their outer edges to a maximum value near their centres (Fig. 5), are consistent with a tuned response from thin layers containing CO_2 which thicken from zero at their outer edge to a maximum in the axial part of the plume, within the structural closure. Moreover the highest amplitudes are encountered in the central parts of the most areally extensive horizons. Chadwick *et al.* (2004) have used amplitudes to map thickness variations in the CO_2 layers of less than a metre or so.

Plume development

The time-lapse seismic data acquired so far show no evidence that the CO_2 repository is leaking. The topmost accumulation of CO_2, corresponding to Horizon 9, is trapped at the top of the reservoir, directly beneath the thick, overlying Nordland Shale caprock. At the time of the 1999 survey the CO_2 had just reached the top of the reservoir, with Horizon 9 comprising two small separate accumulations (Fig. 5). By 2001 the separate accumulations had coalesced into a single larger unit that had expanded laterally beneath the seal. A marked north-trending linear prolongation in Horizon 9 (Fig. 5) corresponds to a ridgelike feature at the top of the reservoir. The rapid advance of the CO_2 front along this feature suggests a highly permeable zone, perhaps related to channelling.

Comparing the 1999 and 2001 horizons (Fig. 5), the overall growth of the plume is clear. Most of the horizons have increased in area by lateral expansion, accompanied presumably by a general layer thickening. The uppermost horizons show the largest relative growth, with Horizon 9 showing a near-eightfold increase in area. Downwards through the plume, relative increases show a generally declining trend, with Horizon 1, at the base of the plume, showing a negligible increase in area. Overall plume development therefore is concentrated towards its top, particularly in the upper two CO_2 layers. The middle and lower parts of the plume are also growing, but relatively more slowly. The lowest layer (Horizon 1) seems to

have approached a state of dynamic equilibrium. The most likely explanation for this is that its area has grown to a critical size, such that the component of CO_2 leaking through its overlying seal has increased sufficiently to balance the input of CO_2 from below. A corollary of this is that the thin mudstone layer above the CO_2 may be permeable. Thus, while the main chimney (Fig. 4) is interpreted as the principal feeder of CO_2 into the laterally expanding horizontal layers, there is likely to be vertical leakage through the intra-reservoir mudstones as well. Moreover, some of the interpreted horizons form small, isolated, outliers (Fig. 5) and cannot have been fed directly from the main chimney. Horizon 6, for example, is clearly sourced from the directly underlying northeastern part of Horizon 5 (Fig. 5), presumably by a subsidiary vertical conduit, indicating local enhancement of permeability in the intra-reservoir mudstone beds.

Plume reflectivity has developed in a rather more complex way from 1999 to 2001. In the uppermost part of the plume, Horizon 8, for example, shows increased absolute amplitudes. This is the classic response of a tuned wavelet to layer thickening. At intermediate levels in the plume, reflection amplitudes stay fairly constant, Horizon 5 showing areal increase but with similar peak amplitudes. In the lowest parts of the plume, reflection amplitudes actually decrease somewhat from 1999 to 2001, with Horizon 1 showing a clear shift towards lower amplitudes. The overall reflectivity of the 2001 and 1999 plumes can be compared by subtracting the 1999 signals from the 2001 signals (Fig. 7). In the upper plume (Fig. 7a) reflection amplitudes generally increase, especially in the outer parts, where lateral expansion of the upper layers between 1999 and 2001 was accompanied by layer thickening and, in places, occupation of previously virgin aquifer. In the more axial parts of the upper plume, roughly uniform or slightly reduced amplitudes are consistent with layer thicknesses having reached (and possibly locally exceeded) the tuning thickness. In the lower plume (Fig. 7b) the development of reflectivity is different. The outer parts of the layers still show a slight increase in reflectivity, due presumably to layer thickening, but in the axial part of the lower plume there is a marked decrease in overall reflectivity.

Possible causes of this amplitude decrease include:

(1) Destruction of the stack response. Increasing lateral velocity variation within the plume will decrease the coherence of the CMP stack.

(2) Signal loss due to transmission loss at reflective interfaces, elastic attenuation, or ray-bending/focusing effects. Proper quantification of these effects requires elastic modelling of the pre-stack data however.

(3) Decrease in reflectivity of the individual CO_2 layers due to increased amounts of intra-layer CO_2 at low saturations. This may well be significant; as discussed below, a portion of the CO_2 is likely to exist in this form, concentrated in the central, axial part of the plume.

(4) Decrease in thickness of the CO_2 layers leading to attenuation of the tuning wavelet. Whilst this may be specifically applicable to the lowest horizon, it does not seem to be consistent with the increasing areas of the other horizons and can therefore be discounted as a general effect.

Velocity pushdown

The lowering of seismic velocity due to the presence of CO_2 (Fig. 3) produces a prominent pushdown of reflections both within and, particularly, beneath the CO_2 plume (Fig. 8a). By comparing the base of the Utsira Sand on the 1994 baseline and the 1999 and 2001 surveys, it is possible to map the velocity pushdown beneath much of the CO_2 plume. Some uncertainty arises in the axial parts of the plume where reflections on the 1999 and 2001 data are locally degraded, and also beneath the outer parts of the plume where pushdown values are small. Alternatively, the pushdown can be mapped by cross-correlating a window of the sub-plume reflections on the 1994 survey with the same window on the 1999 and 2001 surveys. Picking the cross-correlation peak (Fig. 8b) yields a pushdown time-lag for each seismic trace. Pushdown values derived in this way are particularly stable beneath the outer parts of the bubble, but high pushdown values directly beneath the main CO_2 chimney are not well resolved. Optimized pushdown maps from 1999 and 2001, combining both mapping methods (Fig. 8c), show the pushdown anomalies to be elliptical in plan, similar, though by no means identical, in form to the integrated amplitude plots of the plumes (Fig. 4b). The 1999 pushdown is widely in excess of 20 ms beneath the central parts of the plume and locally more than 40 ms above and east of the injection point. The 2001 pushdown is considerably larger, widely in excess of 30 ms and locally more than 60 ms above and east of the injection point. Notwithstanding uncertainties in detail, the overall form of the pushdown is considered to be robust. It closely follows the form of the CO_2 plume itself (*cf.* Figs 4b and 8c) and is notably

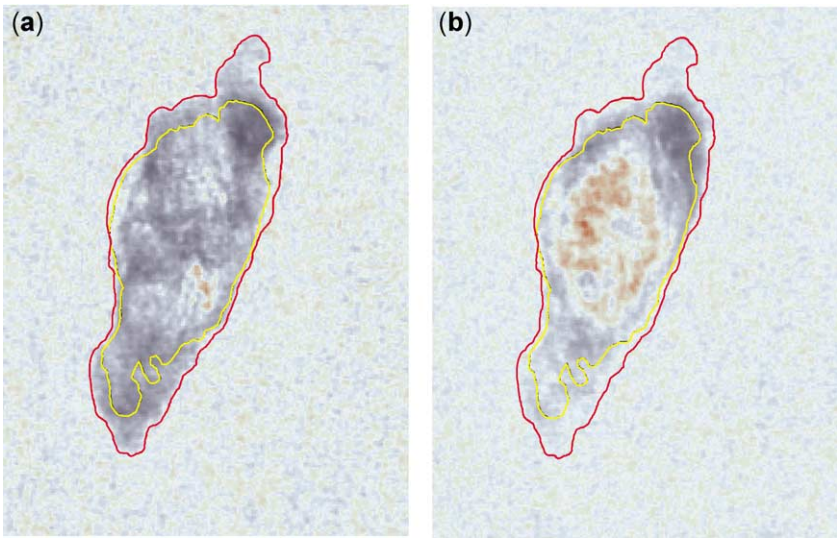

Fig. 7. Plume development 1999–2001. Mean absolute reflection amplitudes in 2001 minus mean absolute amplitudes in 1999 (**a**) Upper plume (850–980 ms twtt window). (**b**) Lower plume (980–1080 ms twtt window). Blue denotes amplitude increase from 1999 to 2001, red denotes amplitude decrease. Yellow and red polygons denote the footprints of the picked seismic horizons in 1999 and 2001 respectively.

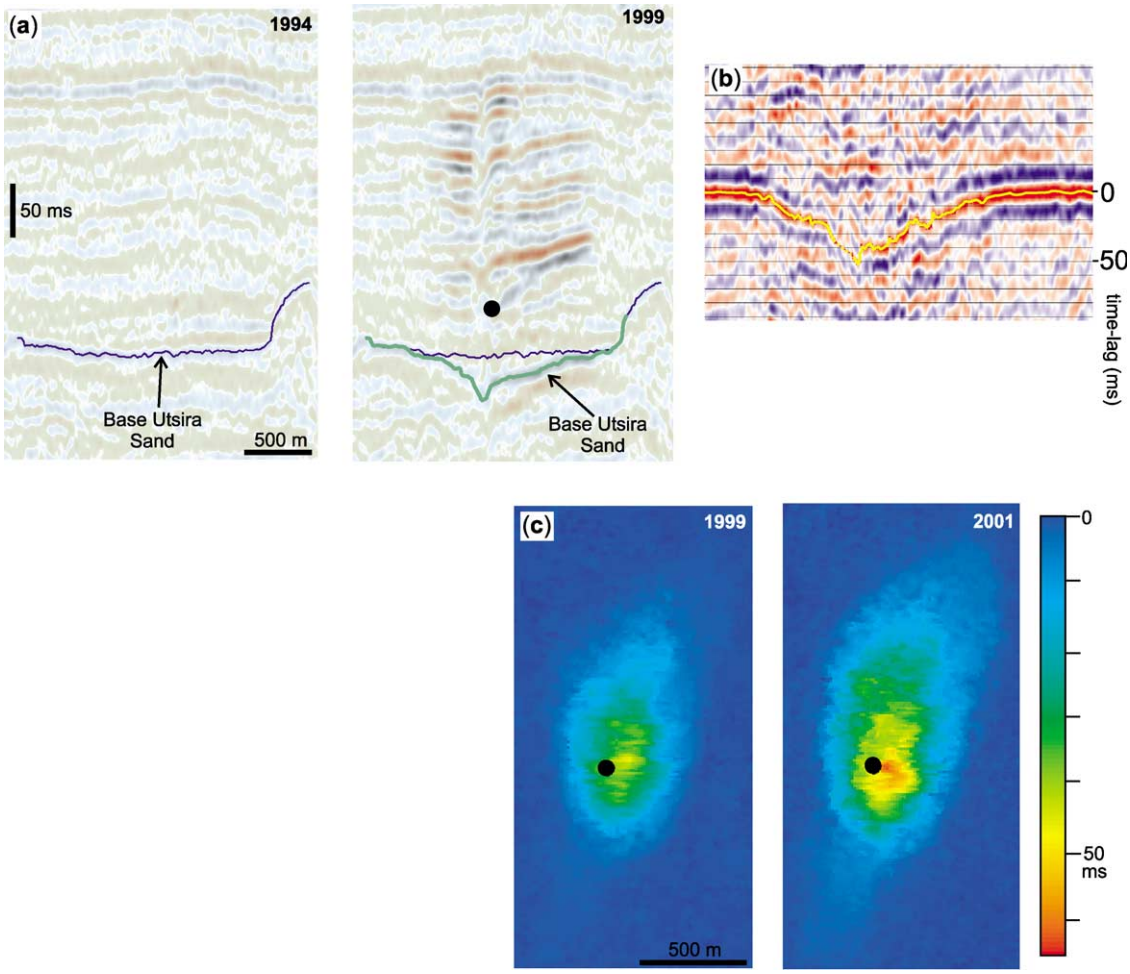

Fig. 8. Velocity pushdown. (**a**) Inline through the reservoir in 1994 and 1999 showing pushdown of the Base Utsira Sand beneath the plume. (**b**) Cross-correlogram of a reflection window beneath the central part of the 2001 plume. Pick follows the correlation peak and defines the pushdown. (**c**) Pushdown maps in 1999 and 2001. Black disc denotes injection point.

similar on both near-, full- and far-offset stacks, the latter showing some smoothing beneath the edges of the plume. The data are, therefore, considered to be reasonably representative of the zero-offset situation, and effects of velocity lensing and injection-induced reservoir compaction as described by Malme *et al*. (2003) and Stammeijer & Landrø (2003) are not considered to be significant. In particular, compaction is unlikely to have occurred as reservoir pressures do not seem to have changed during the injection process.

A CO_2 saturation model of the 1999 plume

A viable plume saturation model has three necessary requirements to satisfy the seismic data: first that it can predict the observed reflectivity; second that it can produce the observed velocity pushdown; and third that the total volume of CO_2 in the model matches the known injected volume, within the limits of parameter uncertainty.

Earlier work (Arts *et al*. 2002; Lygren *et al*. 2002; Chadwick *et al*. 2004) has shown that whilst the plume reflectivity can be explained by CO_2 present in thin layers, the velocity pushdown observed beneath the plume is far too large for the known *in situ* amount of CO_2 to be present only at high saturations. A significant component of lower saturation, or diffuse, CO_2 is also required, a key point being that relatively small volumes of CO_2 at low saturations produce large amounts of pushdown. By examining some illustrative plume saturation models, Chadwick *et al*. (2004) have concluded that the total amount of pushdown may be explained by a model in which CO_2 is partitioned into two components: a main component of high-saturation CO_2 trapped in thin reflective layers (assumed to be trapped beneath the intra-reservoir mudstones), and a lesser component of low-saturation CO_2, dispersed in between the layers, but concentrated towards the axial part of the plume.

We now aim to develop this idea further by building a saturation model for the CO_2 plume that is explicitly matched to both the observed reflectivity and to the velocity pushdown. Our procedure is summarized below:

(1) calculate a thin-layer model for the high saturation CO_2;
(2) calculate the velocity pushdown due to the CO_2 in 1;
(3) subtract the pushdown in 2 from the observed pushdown to obtain the residual pushdown;
(4) calculate an inverse model for the low-saturation diffuse CO_2, mapped to the residual pushdown;
(5) compute the total volume of CO_2 in the combined model;
(6) construct a synthetic seismic model from the saturation model and compare with the observed seismic data.

Thin layer summation for the high saturation component of CO_2

As shown above, the reflectivity of the plume can be explained in terms of thin-layer reflectivity whereby the reflection amplitude can be related directly to layer thickness (Fig. 6).

Assuming that the maximum amplitudes observed in the plume correspond to the tuning thickness of 8.2 m, and making a simplifying linear interpolation, amplitude can be scaled directly to layer thickness for each horizon. For example, in the layer corresponding to Horizon 5, maximum amplitudes are comparable to the highest amplitudes observed in the plume, so its estimated maximum thickness approaches 8 m (Fig. 9a). Scaling directly from amplitude to thickness does however introduce an artefact that affects most of the layers. This is related to the main vertical feeder chimney (and a smaller feature to the east) whereby low seismic amplitudes within these features (e.g. Fig. 4b), give falsely low calculated thicknesses. This is manifest as a prominent 'bulls-eye' around the main chimney (Fig. 9a), where a rim of high thickness values surrounds an area of near zero values within the chimney. This 'chimney effect' was corrected for the layers by simple smooth interpolation across the chimney (subsequent maps in Figure 9 incorporate this interpolated correction).

The capillary pressure, p_c, between the formation brine and the injected CO_2 will cause the CO_2 saturation, S_{CO_2}, to vary with height, h, in each CO_2 layer. The gradient can be computed by balancing the buoyancy, $\Delta\rho gh$, with the capillary pressure.

In SI units:

$$\Delta\rho gh = p_c = 810.35(1 - S_{CO_2})^{-0.948} \quad (1)$$

The capillary pressure–saturation relationship was determined by centrifuge experiments on core material from the Utsira Sand (SACS, unpublished data). The variation of S_{CO_2} with h was thereby computed and, from this, the average value of S_{CO_2} for a range of layer thicknesses (Fig. 10). This relationship was used to map average saturations across each layer (*e.g.* Fig. 9b). Multiplying average CO_2 saturations by layer thicknesses and by average porosity, gives net CO_2 thicknesses for each layer (e.g. Fig. 9c). Summation of these net thicknesses for all the layers gives a first-order estimate of the total amount of CO_2 imaged

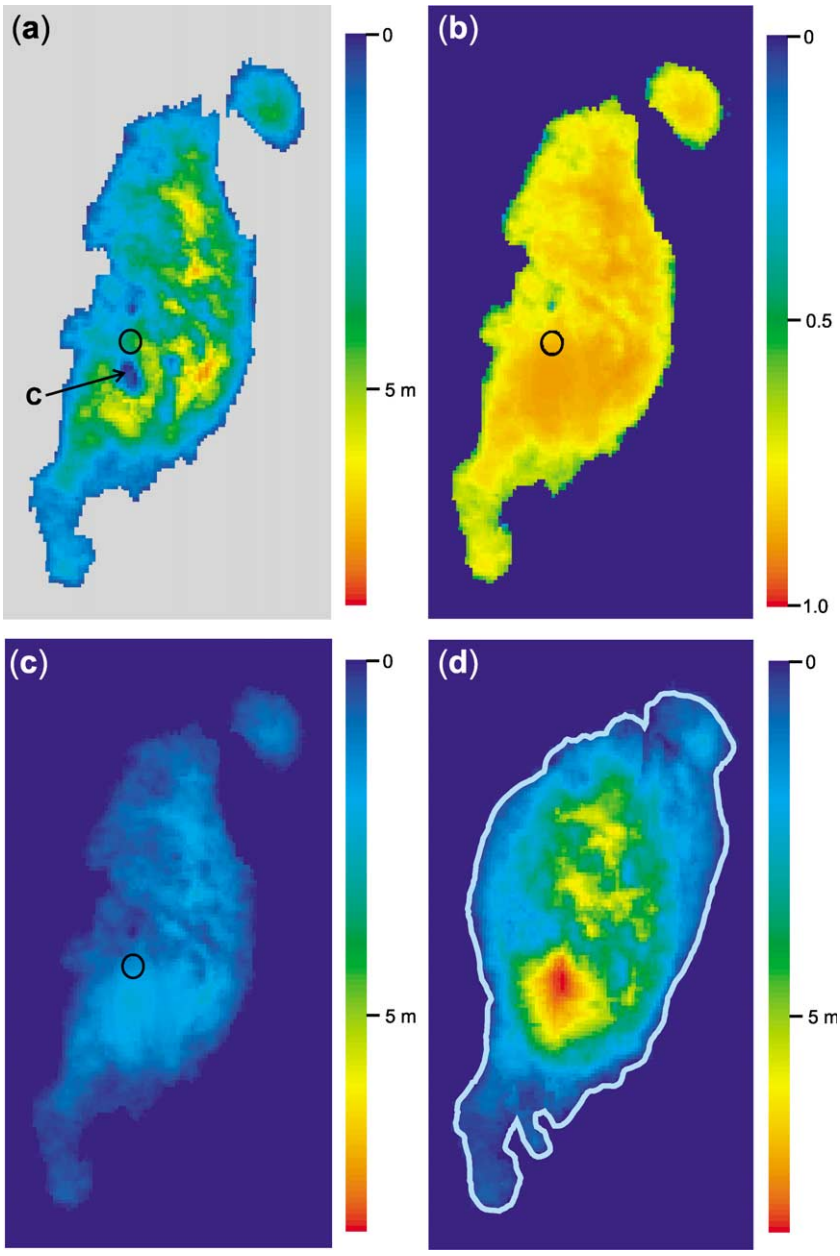

Fig. 9. Thin layer analysis in the 1999 plume. (**a**) Horizon 5 layer thickness (showing thickness artefact around main chimney). (**b**) Horizon 5 CO_2 average saturations. (**c**) Horizon 5 net CO_2 thicknesses. (**d**) Total net CO_2 thickness summed over all the layers. Note (b), (c) and (d) incorporate interpolated smoothing across the chimneys. C denotes the main chimney. Circle denotes injection point. Blue polygon denotes footprint of the picked seismic horizons in the 1999 plume.

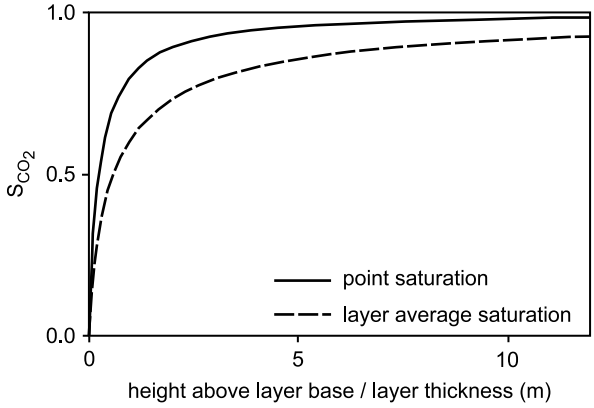

Fig. 10. Variation of CO_2 saturation with layer thickness.

by the seismic data (Fig. 9d). For the interpretation presented here, the total volume in thin layers is about $2.43 \times 10^6\,m^3$, that is about 72% of the estimated injected volume. A number of factors however, alone or in combination, will contribute to uncertainty in this figure. These include uncertainty in the horizon interpretation (including interference between adjacent tuning wavelets), errors in the simple amplitude to thickness conversion, and attenuation of reflectivity in the deeper and axial parts of the plume (see above).

Velocity pushdown

For zero-offset seismic data the velocity pushdown at any point can be related to an overlying column of CO_2 by:

$$\Delta T = \frac{2(V_{SW} - V_{SCO_2})Z}{(V_{SW}V_{SCO_2})} \qquad (2)$$

where ΔT is the time delay at each seismic trace ($T_{99\ \text{survey}} - T_{94\ \text{survey}}$); V_{SW} is the seismic velocity of water-saturated rock; V_{SCO_2} is the seismic velocity of the rock–water–CO_2 column; Z is the thickness of the overlying rock–water–CO_2 column.

The expression below is defined as the Gross Pushdown Factor (GPF):

$$\frac{2(V_{SW} - V_{SCO_2})}{(V_{SW}V_{SCO_2})}.$$

The GPF has units of sm^{-1} and gives the amount of pushdown in seconds (or, more conveniently, milliseconds), produced per metre thickness of a rock–water–CO_2 column. It varies directly with CO_2 saturation and ranges from zero in water-saturated rock, to about 0.45 milliseconds per metre at high CO_2 saturations (Fig. 3).

Velocity pushdown for the high saturation component of CO_2

For each of the interpreted horizons, the average CO_2 saturation at every grid point (e.g. Fig. 9b) was used to calculate the seismic velocity and the GPF (Fig. 3). The GPF was then multiplied by the layer thickness to give the pushdown at each grid point. Pushdown maps were thereby obtained for all the layers. The layer corresponding to Horizon 5 for example produces about 3 ms of pushdown in its thickest part (Fig. 11a).

Summation of the pushdowns for the individual layers gives the total velocity pushdown for the high saturation component of CO_2 in the plume (Fig. 11b). This varies quite smoothly across the plume, generally between about 4 and 8 ms, and increasing towards about 12 ms around the main chimney.

It is clear that the amount of pushdown attributable to high saturation CO_2 is much lower than the total observed pushdown, the latter peaking at more than 40 ms (Fig. 11c). This discrepancy forms a central tenet of the paper and is worth some further discussion. Layer-related pushdown could be increased either by reducing layer velocities or by increasing layer thicknesses. Uncertainties in the former (e.g. Chadwick *et al.* 2004) seem insufficient to significantly reduce the discrepancy. Although the amplitude–thickness (tuning) relationship seems well-founded, potential uncertainty may lie in the calculated layer thicknesses however. If reservoir temperatures were significantly higher than assumed, the total volume of CO_2 in the reservoir could be higher by between 50 and 100%. This would allow layer thicknesses to increase in proportion (the tuning relation would of course no longer hold). Such a change could produce layer-related pushdown in the order of 20–30 ms, probably still significantly below the observed values. Work currently in progress is aimed at providing further, independent constraints on absolute layer thicknesses.

Velocity pushdown for the low saturation, diffuse component of CO_2

By subtracting the calculated layer pushdown from the observed pushdown, the residual plume pushdown is obtained (Fig. 11d). This is concentrated markedly in the axial parts of the plume, and peaking at over 30 ms, it comprises the greater part of the observed pushdown.

An inverse model for the low saturation, diffuse component of CO_2

That part of the plume available to be occupied by the diffuse component of CO_2 is here termed the 'residual plume', and can be defined by isopachs of the plume envelope between the top of Horizon 9 and the top of Horizon 1 (the latter assumed to be flat), with the thickness of Horizons 2 to 9 subtracted (Fig. 12a). The GPF for the residual plume (Fig. 12b) can be obtained directly by dividing the residual pushdown by the residual isopach (Equation 2). The GPF corresponds closely to the residual pushdown (Fig. 11d) and varies from nearly 0.3 milliseconds per metre in the axial parts of the plume to zero in its outer parts (scattered high values near the outer plume edge represent 'noise' where very small residual pushdowns are divided by near-zero residual thicknesses).

The calculated GPF at each grid point effectively integrates the properties of the whole thickness of the residual plume, so only a vertically averaged value of CO_2 saturation can be obtained from the GPF. In line with this limitation, we vary saturation laterally from edge to centre but not vertically. The latter assumption represents the simplest possible CO_2 distribution and clearly is unlikely to be strictly true, but the observation that pushdown develops downwards through the plume in a fairly linear manner supports the broad contention. With these constraints, saturation can be computed directly from the GPF via the Gassmann relationships (Fig. 3). Calculated saturations in the residual plume (Fig. 12c) vary from nearly 0.1 in the axial parts of the plume to less than 0.01 in its outer parts. The total net thickness of CO_2 in the residual plume (Fig. 12d) can be computed by multiplying the saturation by the residual plume isopach (Fig. 12a) and by the average porosity. Net thicknesses are close to zero in the outer parts of the residual plume, but increase gradually inwards to more than 3 m the axial parts (note that the scattered noisy gridpoints seen on the GPF and saturation maps are reduced to insignificance by virtue of being multiplied by near-zero residual isopach values). Integrating this thickness distribution over the area of the plume gives a total volume of CO_2 in the residual plume of $0.44 \times 10^6\,m^3$, about 13% of the known injected volume.

Calculating the total volume of CO_2

Summation of the high-saturation CO_2 trapped in thin layers (Fig. 13a) and the diffuse CO_2 occupying the residual plume

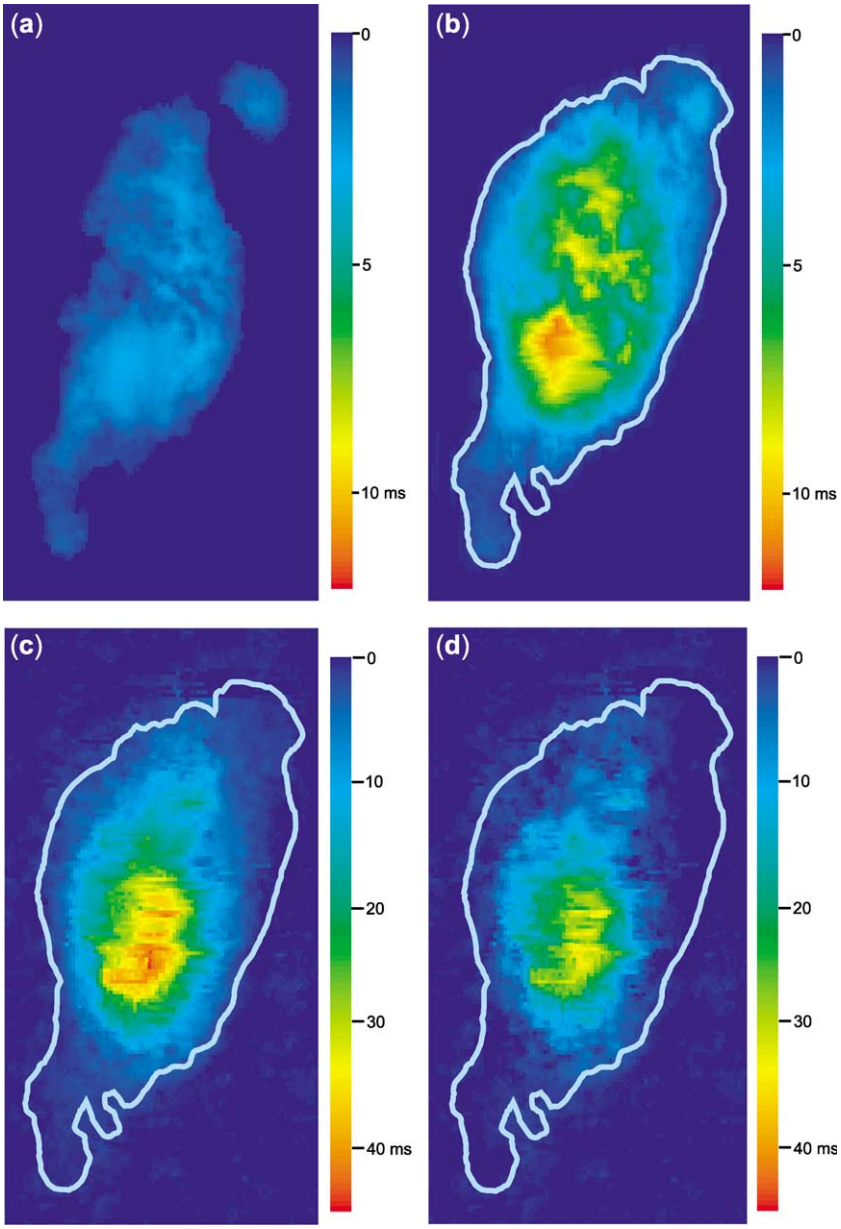

Fig. 11. 1999 velocity pushdown. (**a**) Calculated pushdown due to an individual layer (Horizon 5). (**b**) Calculated total pushdown due to CO_2 trapped in all layers. (**c**) Observed pushdown. (**d**) Residual pushdown. Blue polygon denotes footprint of the picked seismic horizons in the 1999 plume. Note colour scale in (a) and (b) differs from scale in (c) and (d).

(Fig. 13b), gives the total amount of CO_2 *in situ* (Fig. 13c). The total amount of CO_2 in the model is $2.87 \times 10^6\,m^3$. At the assumed CO_2 density of $700\,kgm^{-3}$ (Table 1) this corresponds to $2.01 \times 10^9\,kg$, some 85% of the known injected mass of $2.35 \times 10^9\,kg$.

A synthetic seismic model of the saturation model

In order to test further the validity of the saturation model, a 2D convolutional synthetic seismic section was generated along a west–east cross-line (Fig. 14). The starting model, with acoustic parameters from Table 1, comprises a sandy reservoir unit varying in thickness between 217 and 276 m. Within this, six mudstone beds, each 1 m thick, correspond roughly to Horizons 1, 2, 3, 4, 5 and 7. The 'five-metre mudstone' (Fig. 2) was placed 16 m beneath the reservoir top and corresponds to the top of Horizon 8 (Horizons 6 and 9 do not appear on the line of section). As discussed above, the data do not fully resolve bedding geometries in the reservoir, so for simplicity the thin mudstone beds were assumed to be flat. The synthetic seismogram of the pre-injection model (Fig. 14a) is similar to the observed data (Fig. 14d). It is notable that the thin mudstone beds are visible as faint tuned wavelets, whereas they are more-or-less obscured by noise on the real data. The situation where CO_2 is present just as high-saturation layers (extracted from the layer thickness grids) is modelled first (Fig.14b). The synthetic reflection amplitudes closely match the observed data (Fig. 14e), but the velocity pushdown both within the plume and at base reservoir level is insufficient. Adding the low-saturation component of CO_2 into the residual plume (Fig. 14c) produces the necessary pushdown, and broadly reproduces the observed reflectivity.

Differences of detail between the observed and synthetic datasets serve to illustrate the nature of the main uncertainties. Higher layer reflectivity in the axial part of the real plume is consistent with diffuse CO_2 saturations being patchy rather than homogeneous as was assumed in calculating the velocities from the Gassmann equations. Synthetic velocity pushdowns within the plume are generally somewhat larger than observed. This may highlight a deficiency in the simplifying assumption of vertically uniform saturation in the residual plume. Alternatively, it may just

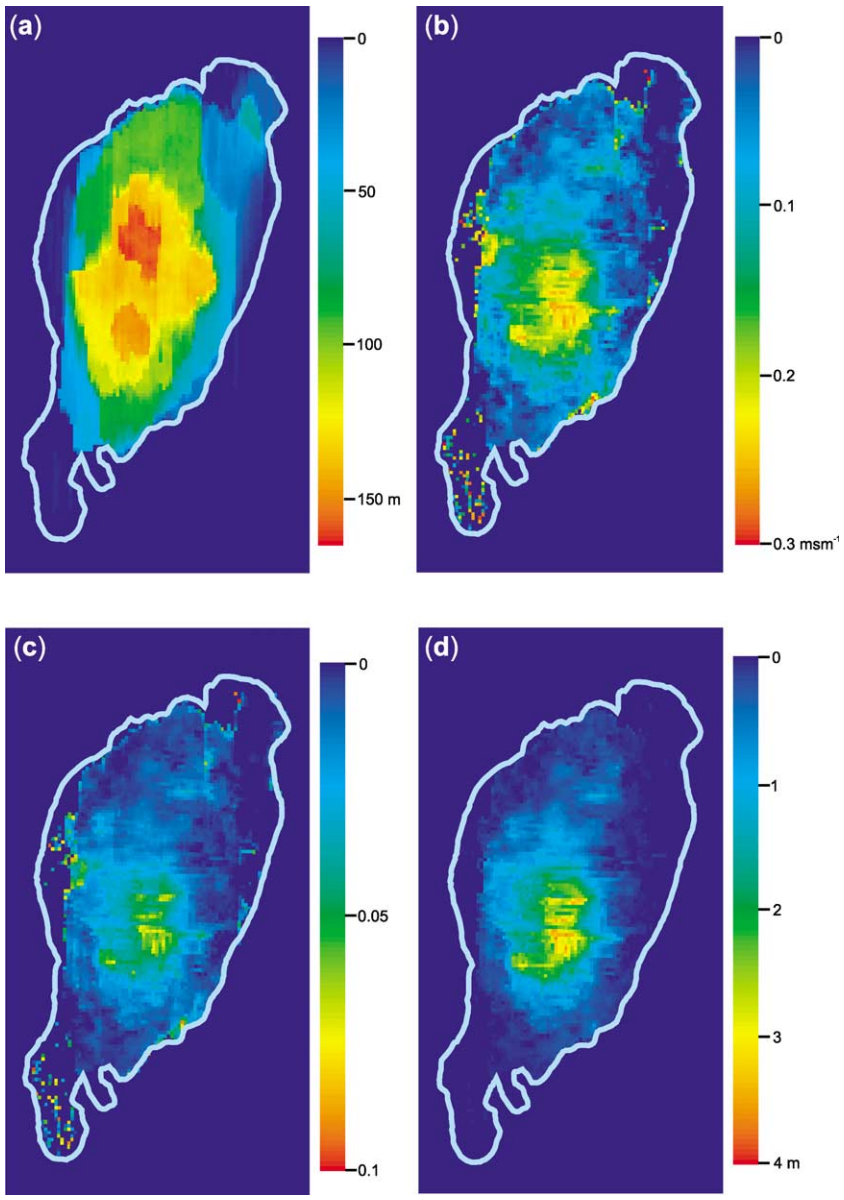

Fig. 12. Calculating the diffuse component of CO_2 within the residual plume. (**a**) Isopachs of the residual plume (top Horizon 1 to top Horizon 9, minus layer thicknesses). (**b**) Gross Pushdown Factor in the residual plume. (**c**) CO_2 saturation. (**d**) Net CO_2 thickness. Blue polygon denotes footprint of the picked seismic horizons in the 1999 plume.

be an effect of the assumed horizontal layering in the model, compared to possible antiformal geometry in the real reservoir. The thin-layer model predicts reflectivity that comprises dominantly tuning wavelets (Fig. 6), with characteristic opposed polarity doublet signatures (Fig.14b,c). The observed data, however, show a mixture of doublets and near-zero phase symmetrical wavelets (Fig. 14e). This suggests additional complexity of internal plume structure, perhaps, for example, involving more gradational layer lower boundaries than indicated by the capillary-height function.

Discussion and conclusions

We have demonstrated that time-lapse seismic monitoring can be used to quantify the amount of CO_2 *in situ.* The model developed here for the 1999 plume assumes that the CO_2 is partitioned between a major, high saturation component trapped as thin layers and a lesser, low-saturation component held in more diffuse form in between the layers. Chadwick *et al*. (2004) have shown that the ratio of velocity pushdown to plume reflectivity is much higher in the axial parts of the plume than at its edges, consistent with the presence of diffuse CO_2 in the axial region. Arts *et al.* (2003, 2004) plotted seismic amplitudes against velocity pushdown in various parts of the plume. The outer parts of the plume, where only a single layer of high saturation CO_2 is present, obey the thin-bed tuning relationship (Fig. 6), whereas in the axial parts of the plume pushdown values are much higher for a given cumulative seismic amplitude, again suggesting the presence of lower saturation CO_2. Low-saturation CO_2 in the residual plume is presumably a consequence of upward percolation from the layers through the overlying mudstone beds, which may be semi-permeable. The permeability could either be on a microsopic scale or could arise as a consequence of stochastically distributed small holes, perhaps resulting from sedimentary processes such as sand intrusion. Reservoir flow simulations do indicate, however, that extensive clouds of diffuse CO_2 are difficult to produce, due the low mobility of CO_2 at low saturations (Erik Lindeberg, pers. comm.). This suggests that the low-saturation component may not be as uniformly distributed through the residual plume as suggested by the model. One way of assessing this would be to map velocity pushdown at a number of levels within the plume, and from this derive a vertical saturation profile in the residual plume.

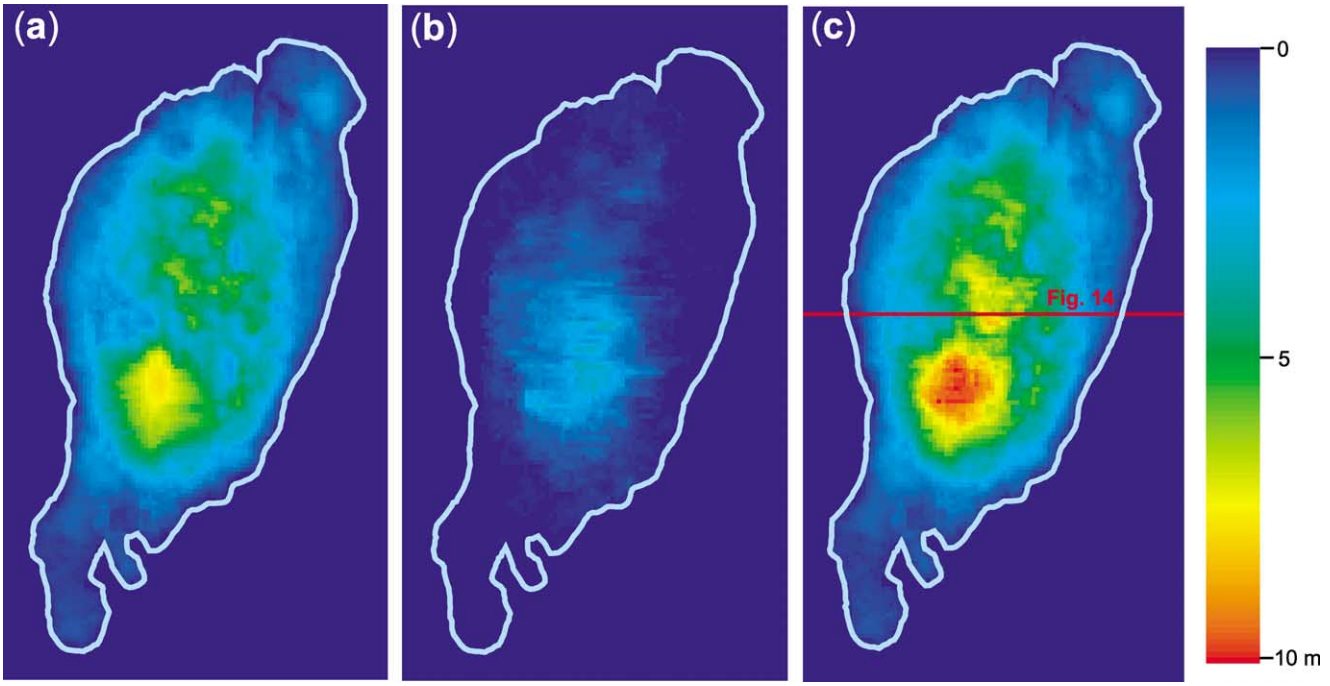

Fig. 13. Calculating the total amount of CO_2 in the plume saturation model. (**a**) Corrected total net CO_2 thickness in the layers. (**b**) Net CO_2 thickness in the residual plume. (**c**) Total net CO_2 thickness in the layers and the residual plume. Blue polygon denotes footprint of the picked seismic horizons in the 1999 plume.

Unfortunately this presents a considerable technical challenge as the pre-injection reservoir bedding geometry is not well constrained.

Our model has a calculated CO_2 mass of 2.01×10^9 kg, which represents over 85% of the known injected mass. Assuming, as discussed above, that no detectable amount of CO_2 has actually escaped from the reservoir, the shortfall of less than 15% can be attributed to a number of factors. A potentially important process is the dissolution of CO_2 into the formation water, whereby it becomes seismically invisible. Dissolution rates are poorly constrained, depending on the dynamic surface area of the CO_2 plume exposed to water and, by inference, the amount of low-saturation diffuse CO_2 (Lindeberg *et al*. 2001; Lindeberg & Bergmo 2003). Simulations of Sleipner by Johnson & Nitao (2003) predict that between 15% and 20% of the free CO_2 will have dissolved after ten years' injection. In 1999, after only three years' injection, amounts dissolved are likely to be small and therefore probably less than 5%. In addition to dissolution effects, three specific uncertainties are likely to have contributed to the calculated mass shortfall. Firstly, the probable incomplete resolution of the short-wavelength pushdown peak associated with the main chimney would result in insufficiently high CO_2 saturations being mapped within the chimney in the residual plume. Secondly, the assumption of a vertically uniform saturation profile in the residual plume effectively produces the minimum saturation compatible with the residual pushdown. If, as suggested above, the diffuse CO_2 were concentrated at certain levels, or in a patchy manner, then more CO_2 would be required in the residual plume to produce the residual pushdown. Thirdly, the presence of low-saturation CO_2 within the axial parts of the plume will tend to reduce the reflectivity of the thin layers and, consequently, the calculated layer thicknesses. Other uncertainties are more-or-less unbiased with respect to mass estimates. For example, potential errors are associated with the thin-bed summation, related to uncertainties in the horizon interpretation and the tuning relationship. More general uncertainties in the acoustic and physical parameters have been quantified by a Monte Carlo simulation, albeit on a single 'mean' saturation model (SACS, unpublished data). The simulations indicate that the shortfall of about 15% has a roughly 50% chance of being entirely attributable to parameter uncertainty. Bearing in mind therefore the likelihood of some loss of free CO_2 due to dissolution, and the nature of the main uncertainties, the current model can be considered therefore to provide a reasonable verification of the *in situ* mass of CO_2.

The quantitative model has been applied to the 1999 dataset, but not yet to the 2001 survey. In principle, similar assumptions can be made, as the layers are still likely to be sufficiently thin for their reflectivity to obey the tuning relationship (see above). However, it is probable that increased amounts of diffuse CO_2 will render the model somewhat less well constrained. An important effect is the loss of reflectivity in the deeper, axial part of the plume (Fig. 7) and also beneath the plume, where velocity pushdown is more difficult to map.

Looking ahead, quantification may well become increasingly difficult with time, through the prograde (injection) phase of plume development (Johnson & Nitao 2003). On cessation of injection, the CO_2 will progressively drain upwards to the caprock, forming the retrograde phase of plume development (Johnson & Nitao 2003). Signal attenuation effects should then gradually dissipate with time, rendering direct seismic quantification of the plume more straightforward. It is, therefore, during its mature prograde phase, that the plume is likely to be most difficult to quantify seismically. More advanced techniques such as pre-stack elastic modelling will have key applications. Pre-stack depth migration has been carried out on the data but results so far have provided limited additional insights due to the difficulty in building a sufficiently precise velocity model. In addition, other, complementary geophysical methods such as microgravimetry may have an important part to play. Theoretical studies (SACS unpublished data) have shown that microgravimetry will be most effective as a mass verification tool, when the plume is at a mature progradational stage. To this end, an initial seabed gravity survey has recently been acquired at Sleipner with repeat surveys planned for the future. Gravity surveying can also provide an independent estimate of the *in situ* CO_2 density, a key parameter in the quantitative analysis.

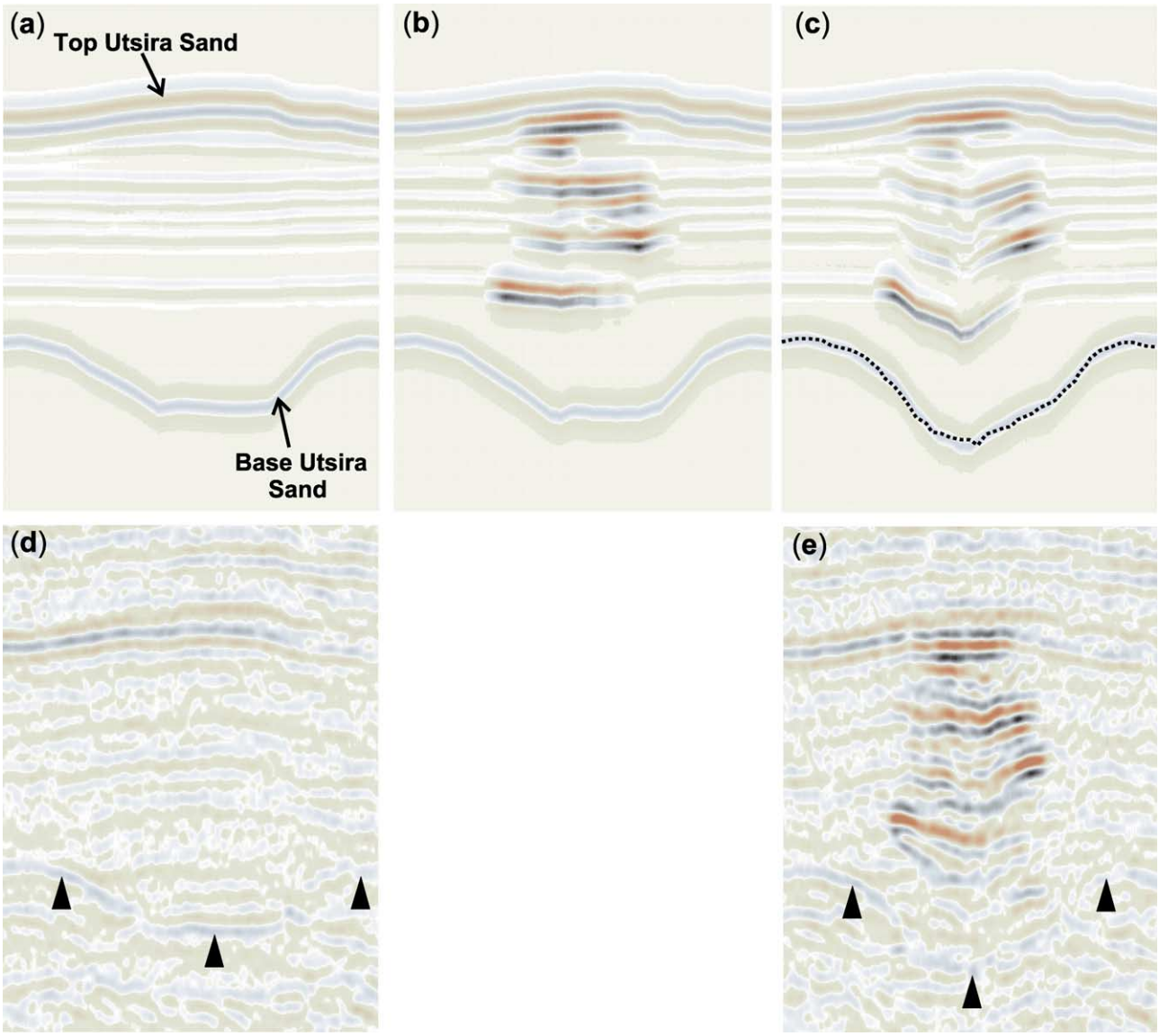

Fig. 14. 2D synthetic seismic modelling along a west–east section through the plume saturation model. (**a**) Synthetic data 1994 prior to injection. (**b**) Synthetic data 1999 with CO_2 layers only. (**c**) Synthetic data 1999 with the full saturation model. (**d**) Observed data 1994 prior to injection. (**e**) Observed data 1999. Arrows indicate Base Utsira Sand on observed data. Dotted line denotes shape of Base Utsira Sand on 1999 observed data, superimposed on 1999 synthetic data.

To conclude, the CO_2 plume at Sleipner is continuing to provide a unique field laboratory for the investigation of CO_2 transport and verification in the subsurface. A saturation model has been developed for the CO_2 plume as observed in 1999. Although with acknowledged limitations, the model reproduces the observed reflectivity and velocity pushdown and provides an acceptable match for the known injected mass.

We thank the SACS and CO2STORE consortia for permission to publish, and also the operators of the Sleipner licence, Statoil, ExxonMobil, Norsk Hydro and Total for their co-operation. Permission to publish is given by the Executive Director, British Geological Survey (NERC). SACS and CO2STORE are funded by the EU Thermie Programme, by industry partners Statoil, BP, ExxonMobil, Norsk Hydro, Total and Vattenfall, and by national governments including the UK Department of Trade and Industry. R&D partners are BGR (Bundesanstalt fur Geowissenschaften und Rohstoffe), BGS (British Geological Survey), BRGM (Bureau de Recherches Geologiques et Minieres), GEUS (Geological Survey of Denmark), IFP (Institute Francais du Petrole), TNO-NITG (Netherlands Institute of Applied Geoscience – National Geological Survey), Schlumberger and SINTEF Petroleum Research. We also acknowledge useful and perceptive reviews by R. Calvert and M. Landrø.

References

Arts, R., Elsayed, R., Van der Meer, L., Eiken, O., Ostmo, S., Chadwick, R.A., Kirby, G.A. & Zinszner, B. 2002. Estimation of the mass of injected CO_2 at Sleipner using time-lapse seismic data. *64th EAGE Conference*, Florence, Paper H-016.

Arts, R., Eiken, O., Chadwick, R. A. Zweigel, P., Van der Meer, L. & Zinszner, B. 2003. Monitoring of CO_2 injected at Sleipner using time lapse seismic data. *In*: Gale, J. & Kaya, Y. (eds) *Greenhouse Gas Control Technologies*. Elsevier, Oxford, 347–352.

Arts, R., Eiken, O., Chadwick, R. A., Zweigel, P., Van der Meer, L. & Kirby, G. A. 2004. Seismic monitoring at the Sleipner underground CO_2 storage site (North Sea). *In*: Baines, S. & Worden, R. J. (eds) *Geological Storage for CO_2 Emissions Reduction*. Geological Society, London, Special Publications, **233**, 181–191.

Baklid, A., Korbøl, R. & Owren, G. 1996. Sleipner Vest CO_2 disposal, CO_2 injection into a shallow underground aquifer. *SPE Annual Technical Conference and Exhibition*, Denver, Colorado, USA, SPE paper, 36600, 1–9

Chadwick, R. A., Holloway, S., Kirby, G. A., Gregersen, U. & Johannessen, P. N. 2001. The Utsira Sand, Central North Sea – an assessment of its potential for regional CO_2 disposal. *In*: Williams, D. J., Durie, R. A., McMullan, P., Paulson, C. A. J. & Smith, A. Y. (eds) *Greenhouse Gas Control Technologies*. CSIRO Publishing, Collingwood, Australia, 349–354.

Chadwick, R. A., Zweigel, P., Gregersen, U., Kirby, G. A., Holloway, S. & Johannessen, P. N. 2003. Geological characterisation of CO_2 storage sites: lessons from Sleipner, northern North Sea. *In*: Gale, J. & Kaya, Y. (eds) *Greenhouse Gas Control Technologies*. Elsevier, Oxford, 321–326.

Chadwick, R. A., Arts, R., Eiken, O., Kirby, G. A., Lindeberg, E. & Zweigel, P. 2004. 4D seismic imaging of a CO_2 bubble at the Sleipner Field, central North Sea. *In*: Davies, R. J., Cartwright, J. A., Stewart, S. A., Lappin, M. & Underhill, J. R. (eds) *3-D Seismic Technology: Application to the Exploration of Sedimentary Basins*. Geological Society, London, Memoirs, **29**, 305–314.

Gassmann, F. 1951. Über die Elastizität poröser Medien. *Vierteljahresschr. der Naturf. Gesellschaft in Zürich*, **96**, 1–23.

Gregersen, U., Michelsen, O. & Sørensen, J. C. 1997. Stratigraphy and facies distribution of the Utsira Formation and the Pliocene sequences in the northern North Sea. *Marine and Petroleum Geology*, **14**, 893–914.

Isaksen, D. & Tonstad, K. 1989. A revised Cretaceous and Tertiary lithostratigraphic nomenclature for the Norwegian North Sea. *Norwegian Petroleum Directory*, Bulletin 5.

Johnson, J. W. & Nitao, J. J. 2003. Reactive transport modelling of geologic CO_2 sequestration at Sleipner. *In*: Gale, J. & Kaya, Y. (eds) *Greenhouse Gas Control Technologies*. Elsevier, Oxford, 327–332.

Lindeberg, E. 1996. Escape of CO_2 from Aquifers. *Energy Conversion Management*, **38**(Suppl), s229–s234.

Lindeberg, E. & Bergmo, P. 2003. The long-term fate of CO_2 injected into an aquifer. *In*: Gale, J. & Kaya, Y. (eds) *Greenhouse Gas Control Technologies*. Elsevier, Oxford, 489–494.

Lindeberg, E., Zweigel, P., Bergmo, P., Ghaderi, A. & Lothe, A. 2001. Prediction of CO_2 distribution pattern by geology and reservoir simulation and verified by time lapse seismic. *In*: Williams, D. J., Durie, R. A., McMullan, P., Paulson, C. A. J. & Smith, A. Y. (eds) *Greenhouse Gas Control Technologies*. CSIRO Publishing, Collingwood, Australia, 372–377.

Lygren, M., Lindeberg, E., Bergmo, P., Dahl, G.V., Halvorsen, K.A., Randen, T. & Sonneland, L. 2002. History matching of CO_2 flow models using seismic modelling and time-lapse data. *Society of Exploration Geophysicists Annual Meeting*, Salt Lake City, October 2002. Extended Abstract.

Malme, T. N., Landrø, M. & Mittet, R. 2003. Effects of overburden distortions on 3D seismic data – a sensitivity study. *EAGE 65th Conference & Exhibition*, Stavanger, Paper C-42.

Pearce, J. M., Czernichowski-Lauriol, I., Rochelle, C. A., Springer, N., Brosse, E., Sanjuan, B., Bateman, K. & Lanini, S. 2001. How will reservoir and caprock react with injected CO_2 at Sleipner? Preliminary evidence from experimental investigations. *In*: Williams, D. J., Durie, R. A., McMullan, P., Paulson, C. A. J. & Smith, A. Y. (eds) *Greenhouse Gas Control Technologies*. CSIRO Publishing, Collingwood, Australia, 355–359.

Span, R. & Wagner, W. 1996. A New Equation of State for Carbon Dioxide covering the Fluid Region from the Triple-Point to 1100 K at Pressures up to 800 MPa. *Journal of Physical and Chemical Reference Data*, 25/6.

Stammeijer, J. & Landrø, M. 2003. Quantitative estimation of compaction and velocity changes using 4D impedance and travel time changes. *EAGE 65th Conference & Exhibition*, Stavanger, Paper A-10.

Zweigel, P., Arts, R., Bidstrup, T., Chadwick, R. A., Eiken, O., Gregersen, U., Hamborg, M., Johanessen, P., Kirby, G. A., Kristensen, L. & Lindeberg, E. 2001. Results and experiences from the first Industrial-scale underground CO_2 sequestration case (Sleipner Field, North Sea). *American Association of Petroleum Geologists*, Annual Meeting, June 2001, Denver, abstract volume (CD).

Zweigel, P., Arts, P., Lothe, A. E. & Lindeberg, E. B. G. 2004. Reservoir geology of the Utsira Formation at the first industrial-scale underground CO2 storage site (Sleipner area, North Sea). *In*: Baines, S. & Worden, R. H. (eds) *Geological Storage for CO_2 Emissions Reduction*. Geological Society, London, Special Publications, **233**, 165–180.